AIP Applied Physics Letters

Direct real space observation of magneto-electronic inhomogeneity in ultra-thin film La0.5Sr0.5CoO3−δ on SrTiO3(001)

S. Kelly, F. Galli, J. Aarts, Shameek Bose, M. Sharma, and C. Leighton

Citation: Applied Physics Letters **105**, 112909 (2014); doi: 10.1063/1.4896283
View online: http://dx.doi.org/10.1063/1.4896283
View Table of Contents: http://scitation.aip.org/content/aip/journal/apl/105/11?ver=pdfcov
Published by the AIP Publishing

Direct real space observation of magneto-electronic inhomogeneity in ultra-thin film $La_{0.5}Sr_{0.5}CoO_{3-\delta}$ on $SrTiO_3(001)$

S. Kelly,[1] F. Galli,[1] J. Aarts,[1,a)] Shameek Bose,[2] M. Sharma,[2] and C. Leighton[2,a)]
[1]*Department of Physics, Leiden University, 2300 RA Leiden, Netherlands*
[2]*Department of Chemical Engineering and Materials Science, University of Minnesota, Minneapolis, Minnesota 55455, USA*

(Received 4 August 2014; accepted 3 September 2014; published online 18 September 2014)

Recent magnetotransport and neutron scattering measurements implicate interfacial magneto-electronic phase separation as the origin of the degradation in transport and magnetism in ultra-thin film $La_{1-x}Sr_xCoO_3$ on $SrTiO_3(001)$. Here, using low temperature scanning tunneling microscopy and spectroscopy the first direct, real space observation of this nanoscopic electronic inhomogeneity is provided. Films of thickness 12.4 nm (32 unit cells) are found to exhibit spatially uniform conductance, in stark contrast to 4.7 nm (12 unit cell) films that display rich variations in conductance, and thus local density of states. The electronic heterogeneity occurs across a hierarchy of length scales (5–50 nm), with complex correlations with both topography and applied magnetic fields. These results thus provide a direct observation of magneto-electronic inhomogeneity in $SrTiO_3(001)/La_{0.5}Sr_{0.5}CoO_3$ at thicknesses below 6–7 nm, in good agreement with less direct techniques. © *2014 AIP Publishing LLC*. [http://dx.doi.org/10.1063/1.4896283]

Degradation in physical properties of "dead layers" at surfaces and interfaces in complex oxide films and heterostructures is well-documented. This phenomenon manifests itself both in heterostructures,[1,2] where the difficulty of maintaining desired properties at interfaces has implications for oxide devices,[3,4] and in single films in the ultra-thin limit,[5–8] where it defines the lowest thickness to which functional phenomena such as ferromagnetism can be maintained. Given the numerous possible mechanisms at work (e.g., electronic and orbital reconstructions,[2,5,9] charge transfer,[2,9] and effects related to strain/defects/chemistry[6–8]), it is important that the origin of this behavior be carefully elucidated in specific systems. Here, we focus on ultra-thin films of the perovskite cobaltite $La_{1-x}Sr_xCoO_3$ (LSCO) on $SrTiO_3(001)$ with low temperature Scanning Tunneling Microscopy (STM).

Perovskite cobaltites are currently investigated for applications as diverse as oxide spintronics,[10] solid oxide fuel cells,[11] and catalysis,[12] and are of much fundamental interest. In the archetypal LSCO, the $x = 0$ bulk parent compound exhibits a low-spin semiconducting ground state and undergoes a thermally-driven spin-state crossover.[13] Bulk Sr doping similarly stabilizes finite spin-states, leading to magnetic clusters, and eventually a uniform long-range ferromagnetic (FM) metal for $x \geq 0.22$.[14–16] Ultra-thin films of LSCO, however, exhibit degraded properties.[10,17] In epitaxial $x = 0.5$ LSCO on $SrTiO_3(001)$, for example (1.8% tensile lattice mismatch), the saturation magnetization and Curie temperature are strongly suppressed below some thickness, t^* (~6–7 nm), accompanied by a metal-insulator transition.[10,17] A clue to the origin of the suppressed magnetization and enhanced resistivity was provided by large, hysteretic, isotropic negative magnetoresistance (MR),[10] reminiscent of the inter-cluster giant MR seen in *low doped* (i.e., $x < 0.22$) bulk LSCO.[18] In such low x crystals, this MR arises from spin-dependent transport between nanoscopic FM metallic clusters in a non-FM insulating matrix, i.e., magneto-electronic phase separation.[14–16,18] Observation of identical MR in ultra-thin films is thus strong evidence that the suppressed magnetization and conductivity result from interface-induced magneto-electronic phase separation, with nanoscopic FM clusters forming in a non-FM insulating matrix near the interface.[10] Limited small-angle neutron scattering data support this, although signal-to-noise issues preclude determination of exact length scales.[10]

The origin of this magneto-electronic inhomogeneity in $SrTiO_3(001)$/LSCO was subsequently elucidated by scanning transmission electron microscopy/electron energy loss spectroscopy (STEM/EELS).[10,19] EELS imaging revealed strong depletion in hole concentration ~10 nm from the $SrTiO_3(001)$ interface, driven by a simultaneous suppression in O content. This O vacancy accumulation was shown to be linked to strain-driven *ordering* of O vacancies. In essence, a novel mechanism for lattice mismatch accommodation occurs, O vacancies forming at low energy cost, and ordering with a modulation vector parallel to the interface in order to expand the in-plane lattice parameter and match the substrate.[10,19] Most recently, the similarity of this O vacancy superstructure to brownmillerite $SrCoO_{2.5}$ was highlighted, and it was shown that the vacancy ordering and depth profile can be manipulated by strain and orientation, raising fascinating prospects for control of transport and magnetism.[19]

While progress with understanding ultra-thin film structure and property degradation in cobaltites has thus been significant, one missing element is direct, real space proof of the purported magneto-electronic inhomogeneity in $SrTiO_3(001)$/LSCO. Indeed, despite the considerable work on magneto-electronic phase separation in bulk [e.g., Refs. 14–16, 18, and 20] and thin film [e.g., Refs. 10 and 17] cobaltites, all studies to date were restricted to reciprocal space, due to the dearth of real space methods to probe electronic and/or magnetic inhomogeneity at such short[14] length scales. Here, we rectify this

a)Authors to whom correspondence should be addressed. Electronic addresses: leighton@umn.edu and aarts@physics.leidenuniv.nl

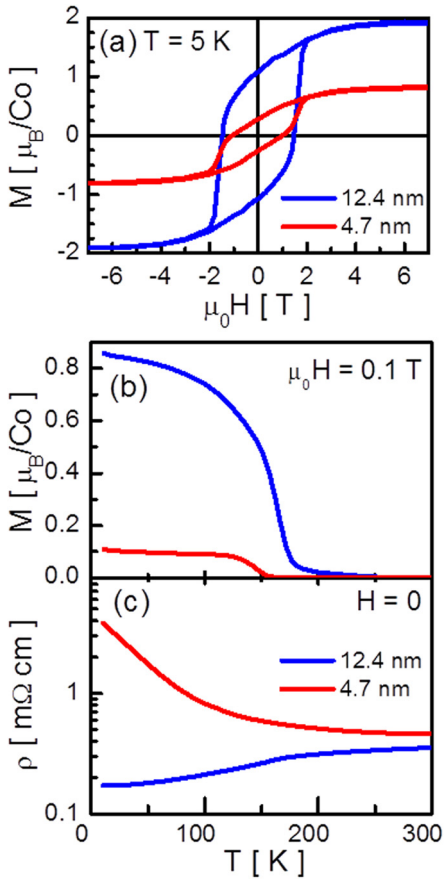

FIG. 1. (a) 5 K hysteresis loops of $SrTiO_3(001)/La_{0.5}Sr_{0.5}CoO_{3-\delta}$ films with thickness 4.7 and 12.4 nm. Temperature dependence of (b) the magnetization in a 0.1 T magnetic field, and (c) zero field resistivity of $SrTiO_3(001)/La_{0.5}Sr_{0.5}CoO_{3-\delta}$ films with thickness 4.7 and 12.4 nm.

by providing the first direct, real space observation of electronic heterogeneity in $SrTiO_3(001)$/LSCO. Low temperature STM and scanning tunneling spectroscopy (STS) have been used to acquire nm spatial resolution conductance maps and current-voltage curves, to probe the local density-of-states (LDOS) at the surface of $SrTiO_3(001)$/LSCO. Films with thickness 12.4 nm (above t^*) are electronically uniform, while films with thickness 4.7 nm (below t^*) reveal strikingly heterogeneous conductance on nanoscopic scales, with complex correlations with topography and applied magnetic field. These results directly verify nanoscale electronic inhomogeneity in ultra-thin film $SrTiO_3(001)$/LSCO.

LSCO $x = 0.50$ films with thickness (from x-ray reflectivity) of $t = 4.7$ nm (12 unit cells) and $t = 12.4$ nm (32 unit cells) were deposited on $SrTiO_3(001)$ from ceramic targets by high-pressure reactive DC magnetron sputtering. Depositions were performed at a substrate temperature ~700 °C, total pressure of 140 mTorr, and O_2/Ar pressure ratio of 0.4, followed by cooling in 500 Torr of O_2 and post-annealing in flowing O_2 at 500 °C. This results in single-phase cation-stoichiometric epitaxial LSCO(001) with optimal oxygenation and properties.[10,17,19,21] Films studied here are below the critical thickness for strain relaxation (20 nm). Following high-resolution x-ray characterization, magnetization (M) and resistivity (ρ) were measured at temperature (T) from 5 to 300 K in magnetic fields ($\mu_o H$) to 7 T. As shown in Fig. 1(a), magnetization hysteresis loops at 5 K reveal clear FM with substantial coercivity,[22] and saturation magnetization that falls from a bulk-like 2 μ_B/Co at $t = 12.4$ nm to 0.8 μ_B/Co at $t = 4.7$ nm. Consistent with prior work,[10,17] we ascribe this not to a uniform reduction in magnetization but to a reduction in FM volume fraction. As shown in Figs. 1(b) and 1(c) this suppression in M is accompanied by a Curie temperature reduction (from ~185 to 150 K), along with a crossover from metallic-like ρ *vs.* T with an inflexion point around the Curie temperature (at $t = 12.4$ nm), to an insulating-like ρ *vs.* T with much larger low T resistivity (at $t = 4.7$ nm). This is consistent with prior work,[10] confirming that these samples straddle the t^* value of 6–7 nm marking the crossover to the proposed electronically and magnetically inhomogeneous state.

STM/STS measurements ($T = 2$–180 K, $\mu_o H \leq 8$ T) were performed using an STM head built in-house and maintained in ultra-high vacuum (UHV, base pressure 3×10^{-10} Torr). After overnight pumping in a load-lock, samples were introduced into the UHV chamber and scanned using mechanically-cut $Pt_{90}Ir_{10}$ STM tips. STS measurements were made at specific locations by sweeping the bias voltage at a fixed sample-tip separation, producing current-voltage (I-V) curves. Differential conductance maps (scanned simultaneously with topography) were measured with a lock-in amplifier using a 10 mV AC modulation at ~1000 Hz. This modulation was superimposed on specified set-point V and I values which serve to fix the sample-tip bias and separation, as illustrated below.

Beginning with the $t = 12.4$ nm film, Fig. 2 summarizes the typical behavior seen by STM/STS at $T = 1.7$ K. To acquire the differential conductance map shown in Fig. 2(a), the tip-sample separation was first fixed by the chosen set-

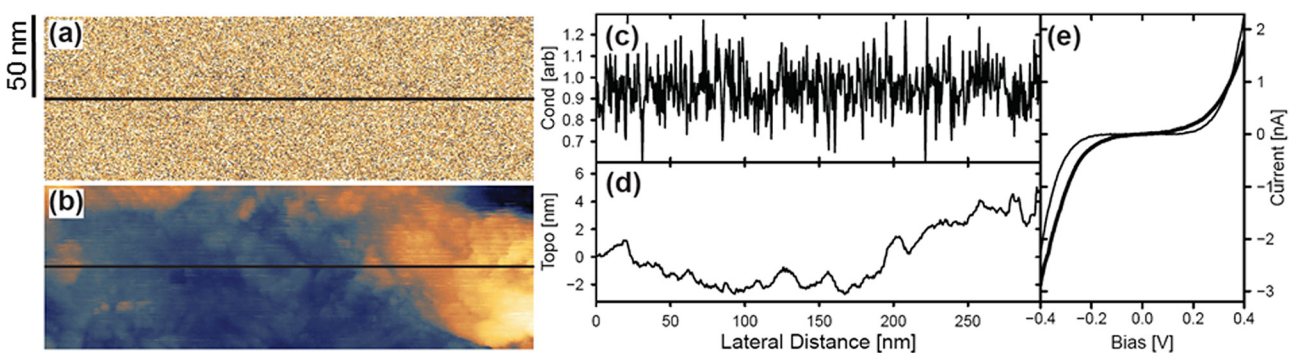

FIG. 2. (a) Differential conductance and (b) corresponding topography (where lighter (yellow) regions are high and darker (blue) regions are low) over a 100 × 300 nm region of a 12.4 nm thick $SrTiO_3(001)/La_{0.5}Sr_{0.5}CoO_{3-\delta}$ film. Data were acquired at 1.7 K with a set-point of 0.6 V and 0.219 nA. Horizontal lines denote the positions of the relative differential conductance and topographic line scans shown in (c) and (d). (e) Two example current-voltage scans taken from a set of 16 measured along a diagonal of a 300 × 300 nm region encompassing the one shown in (a) and (b). Data were acquired with a set-point of 0.35 V and 1 nA.

point (0.60 V bias, 0.22 nA), and the differential conductance about this 0.60 V DC bias probed as a function of position over the 100×300 nm area shown. It is essential to note, as clearly illustrated by the representative *I-V* curves shown in Fig. 2(e), that at these relatively high biases the highest differential conductances are actually associated with the most *insulating* local regions, with the *highest* apparent tunneling gaps, and *lowest* zero bias conductance (ZBC, i.e., the conductance in the zero applied voltage limit). The topographic map acquired simultaneously to this conductance map is shown in Fig. 2(b), while Figs. 2(c) and 2(d) show line scans (along the horizontal lines in Figs. 2(a) and 2(b)) of the relative differential conductance and topography.

The most noteworthy feature is clearly the remarkable uniformity in differential conductance and thus LSCO surface LDOS. There are no obvious contiguous nanoscale areas of similar conductance in Fig. 2(a), and we find no evidence of correlation between conductance (Fig. 2(a)) and topography (Fig. 2(b)), despite the significant root mean square roughness ($\sim$2 nm). This is borne out by the line scans (Figs. 2(c) and 2(d)), which appear uncorrelated, with no systematic changes in conductance where topographical changes occur. Quantifying the conductance fluctuations (Fig. 2(c)) with autocorrelation analysis reveals that correlations are already beneath 95% confidence at lateral scales as short as 0.6 nm. In contrast, the topographic line scan in Fig. 2(d) results in a lateral correlation length of $\sim$50 nm. While the fluctuations in conductance thus must occur on very short length scales, they are indeed present, as confirmed by measurement of *I-V* curves at multiple locations. The curves in Fig. 2(e) are in fact two examples from 16 such curves taken along a diagonal of a 300×300 nm area enclosing the region in Fig. 2(a). 15 of these curves were similar to the fine line in Fig. 2(e), with an average ZBC of 1.4×10^{-2} nA/V and standard deviation 0.8×10^{-2} nA/V. The remaining curve was significantly different (heavy line in Fig. 2(e)), having a ZBC of 3.9×10^{-1} nA/V, i.e., 30$\times$ larger than the average of the other 15. This behavior was found in multiple cases, in several regions, suggesting very small conductance "hotspots." Somewhat similar effects have been seen in otherwise homogeneous manganite films, and attributed to defects.[23]

As shown in Fig. 3, the situation is markedly different in films with thickness 4.7 nm, i.e., below t^*, where we could anticipate the surface to present nanoscale inhomogeneity, reflective of the film interior. In this figure, panels (a)–(c) are representative 55×55 nm differential conductance maps measured at 3.7 K in $\mu_o H = 0$, 4, 8 T, while panel (d) depicts topography. Panels (e) and (f) show scans along the horizontal lines marked on panels (a)–(d), while panel (g) shows representative *I-V* curves at 7.5 K. Again, it is essential to note that in these conductance maps, which were measured at a set-point of 0.70 V and 0.21 nA (comparable to Fig. 2), the highest differential conductances are actually associated with the most *insulating* local regions, with the *highest* apparent tunneling gaps, and *lowest* ZBC, as clearly shown in Fig. 3(g). The dark (blue) regions in Figs. 3(a)–3(c) are thus the most metallic, the light (yellow) areas being more insulating.

The heterogeneity visible in Figs. 3(a)–3(c) is striking. As in prior STM/STS work on electronically inhomogeneous manganites,[24–28] contiguous nanoscale regions of similar differential conductance are evident, conductive clusters forming in an insulating matrix. The extent of this inhomogeneity is reinforced by Fig. 3(g), which shows STS *I-V* curves representative of the dark (blue) and light (yellow) regions. The heavy line (representative of the conductive clusters) has a ZBC of 1.6 nA/V, while the fine line (representative of the insulating matrix) yields a ZBC of 1.4×10^{-2} nA/V, the factor of 120 between the two greatly exceeding the factor of 30 between extremal ZBCs on the thicker film. The 4.7 nm LSCO film thus exhibits much larger fluctuations in conductance and LDOS than the 12.5 nm film, direct confirmation of the deductions discussed in the introduction.

Interestingly, Fig. 3(a) also reveals that the electronic heterogeneity in these ultra-thin films is not on a single

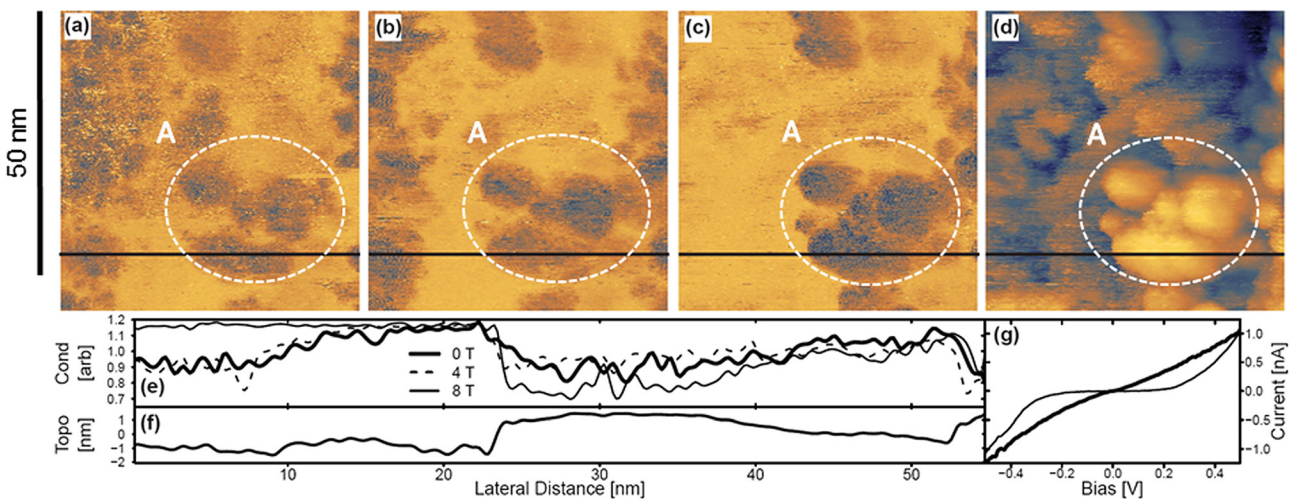

FIG. 3. (a)–(c) Differential conductance and (d) topography (where lighter (yellow) regions are high and darker (blue) regions are low) over a 55×55 nm representative region of a 4.7 nm thick $SrTiO_3(001)/La_{0.5}Sr_{0.5}CoO_{3-\delta}$ film. Data were acquired at 3.7 K with a set-point of 0.7 V and 210 pA, comparable to the maps in Fig. 2. Panels (a)–(c) are differential conductance maps measured in 0, 4, and 8 T magnetic fields, respectively. The horizontal lines denote the positions of the relative differential conductance and topographic line scans shown in (e) and (f). (g) Two example current-voltage scans. Data were taken from a different region to that shown in panels (a)–(d), at 7.5 K, with a setpoint of 0.5 V and 1 nA, comparable to the current-voltage curves in Fig. 2. In the region marked "A" in (a)–(d) topography and conductance correlate, as discussed in the text.

length scale, but instead occurs over a hierarchy of scales from ~5 to 50 nm. Numerous additional images confirm this, occasionally showing even larger metallic clusters, up to 100 nm. As can be seen by comparing Figs. 3(a) and 3(d), the extent to which this electronic texture is correlated with topography is also non-trivial. There are certainly regions (such as the one labeled "A" in Fig. 3), where the conductance and topography are correlated, the more metallic behavior occurring in locally thicker regions. On the other hand, as illustrated by the entire left side of Figs. 3(a) and 3(d), there are also regions with no clear correlation between conductance and height. Further quantification can be achieved with the line scans shown in Figs. 3(e) and 3(f). Abrupt topographical features are indeed accompanied by conductance changes in some cases, e.g., at a lateral distance of 22 nm when region A is entered; correlations between conductance and topography are in fact clear across this whole region (from 22 to 50 nm). On the whole however, the fluctuations in conductance in Fig. 3(e) occur over significantly shorter lateral scales than those in the topography, the lateral correlation length of the $H = 0$ conductance fluctuations being a factor of ~2 smaller than the equivalent value for topography.

As can also be seen from Figs. 3(a)–3(c), comparing 0, 4, and 8 T data, the response to a magnetic field is quite complex and appears to be opposite in different regions. On the entire left side of Figs. 3(a)–3(c) for instance, where the conductance is uncorrelated with topography, magnetic field favors an insulating state. This can be seen by comparing Fig. 3(a) with Figs. 3(b) and 3(c) (where the image gets progressively lighter with increasing H), and by examining the line scans in Fig. 3(e) between 0 and 15 nm. The latter reveals a 25% increase in differential conductance in 8 T, meaning a substantial decrease in ZBC and thus a decrease in metallicity, i.e., local positive magnetoresistance. In contrast, in region A (inside the dashed line in Figs. 3(a)–3(d), and from 22 to 50 nm in Fig. 3(e)), where correlations with topography do occur, the situation is opposite. Applied fields decrease the high bias differential conductance, thus increasing the ZBC and metallicity. This corresponds to a local negative magnetoresistance, which the line scans in Fig. 3(e) show to be a 5%–10% effect in 8 T. These H-dependent STM/STS observations are broadly consistent with conclusions from prior macroscopic magnetotransport. Specifically, the local negative magnetoresistance in the most conductive nanoscopic clusters, and the local positive magnetoresistance in sections of the insulating matrix, are consistent with the interpretation of the macroscopic negative magnetoresistance (−30% under these conditions) in terms of inter-cluster transport. Figs. 3(a)–3(c) also clearly demonstrate the absence of H-induced percolation (highlighting the dissimilarity with colossal magnetoresistance in the manganites), likely due to the essential role played by chemical disorder in electronic/magnetic heterogeneity in LSCO.[14,16]

In summary, STM/STS has been used to probe the surface LDOS in STO(001)/LSCO films with thickness 4.7 and 12.4 nm, spanning the 6–7 nm range where electronic and magnetic heterogeneity have been postulated to set in. The data reveal largely homogeneous conductance in the thicker films, but indeed confirm significant nanoscale electronic inhomogeneity below 6–7 nm. This inhomogeneity occurs across a hierarchy of length scales, mostly concentrated from 5 to 50 nm, and is retained even in large applied fields. Direct, real space verification of electronic heterogeneity as the origin of degraded properties in ultrathin STO(001)/LSCO is thus obtained.

Work at Leiden supported in part by NanoNed, a national nanotechnology program coordinated by the Dutch Ministry of Economic Affairs, and by a research program of the Stichting F.O.M., which is financially supported by the Dutch national science foundation, NWO. Work at UMN supported by NSF (DMR-1206278), and DOE (DE-FG02-06ER46275, specifically scattering characterization).

[1]H. Yamada, Y. Ogawa, Y. Ishii, H. Sato, M. Kawasaki, H. Akoh, and Y. Tokura, Science **305**, 646 (2004).
[2]F. Y. Bruno, J. Garcia-Barriocanal, M. Varela, N. M. Nemes, P. Thakur, J. C. Cezar, N. B. Brookes, A. Rivera-Calzada, M. Garcia-Hernandez, C. Leon, S. Okamoto, S. J. Pennycook, and J. Santamaria, Phys. Rev. Lett. **106**, 147205 (2011).
[3]R. Ramesh and D. G. Schlom, MRS Bull. **33**, 1006 (2008); J. Mannhart, D. H. A. Blank, H. Y. Hwang, A. J. Millis, and J.-M. Triscone, *ibid.* **33**, 1027 (2008); E. Dagotto and Y. Tokura, *ibid.* **33**, 1037 (2008); N. A. Spaldin and R. Ramesh, *ibid.* **33**, 1047 (2008).
[4]J. Chakhalian, A. J. Millis, and J. Rondinelli, Nat. Mater. **11**, 92 (2012).
[5]M. Huijben, L. W. Martin, Y.-H. Chu, M. B. Holcomb, P. Yu, G. Rijnders, D. H. A. Blank, and R. Ramesh, Phys. Rev. B **78**, 094413 (2008).
[6]M. Bibes, L. Balcells, S. Valencia, J. Fontcuberta, M. Wojcik, E. Jedryka, and S. Nadolski, Phys. Rev. Lett. **87**, 067210 (2001).
[7]R. V. Chopdekar, E. Arenholz, and Y. Suzuki, Phys. Rev. B **79**, 104417 (2009).
[8]L. Fitting-Kourkoutis, J. H. Song, H. Y. Hwang, and D. A. Muller, Proc. Natl. Acad Sci. U.S.A. **107**, 11682 (2010).
[9]S. Smadici, P. Abbamonte, A. Bhattacharya, X. Zhai, B. Jiang, A. Rusydi, J. N. Eckstein, S. D. Bader, and J.-M. Zuo, Phys. Rev. Lett. **99**, 196404 (2007).
[10]M. A. Torija, M. Sharma, J. Gazquez, M. Varela, C. He, J. Schmitt, J. A. Borchers, M. Laver, S. El-Khatib, and C. Leighton, Adv. Mater. **23**, 2711 (2011).
[11]M. Kubicek, Z. Cai, W. Ma, B. Yildiz, H. Hutter, and J. Fleig, ACS Nano **7**, 3276 (2013).
[12]C. H. Kim, G. Qi, K. Dahlberg, and W. Li, Science **327**, 1624 (2010).
[13]See the following and references within: D. P. Kozlenko, N. O. Golosova, Z. Jirak, L. S. Dubrovinsky, B. N. Savenko, M. G. Tucker, Y. Le Godec, and V. P. Glazkov, Phys. Rev. B **75**, 064422 (2007).
[14]C. He, S. El-Khatib, J. Wu, J. W. Lynn, H. Zheng, J. F. Mitchell, and C. Leighton, Europhys. Lett. **87**, 27006 (2009).
[15]C. He, S. El-Khatib, S. Eisenberg, M. Manno, J. W. Lynn, H. Zheng, J. F. Mitchell, and C. Leighton, Appl. Phys. Lett. **95**, 222511 (2009).
[16]C. He, S. Eisenberg, C. Jan, H. Zheng, J. F. Mitchell, and C. Leighton, Phys. Rev. B **80**, 214411 (2009).
[17]M. A. Torija, M. Sharma, M. R. Fitzsimmons, M. Varela, J. Wu, and C. Leighton, J. Appl. Phys. **104**, 023901 (2008).
[18]J. Wu, J. W. Lynn, C. Glinka, J. Burley, H. Zheng, J. F. Mitchell, and C. Leighton, Phys. Rev. Lett. **94**, 037201 (2005).
[19]J. Gazquez, S. Bose, M. Sharma, M. A. Torija, S. J. Pennycook, C. Leighton, and M. Varela, APL Mater. **1**, 012105 (2013).
[20]D. Phelan, D. Louca, S. Rosenkranz, S.-H. Lee, Y. Qui, P. J. Chupas, R. Osborn, H. Zheng, J. F. Mitchell, J. R. D. Copley, J. L. Sarrao, and Y. Moritomo, Phys. Rev. Lett. **96**, 027201 (2006); D. Phelan, D. Louca, K. Kamazawa, S.-H. Lee, S. N. Ancona, S. Rosenkranz, Y. Motome, M. F. Hundley, J. F. Mitchell, and Y. Moritomo, *ibid.* **97**, 235501 (2006).
[21]M. Sharma, J. Gazquez, M. Varela, J. Schmitt, and C. Leighton, J. Vac. Sci. Technol. **29**, 051511 (2011).
[22]M. Sharma, J. Gazquez, M. Varela, J. Schmitt, and C. Leighton, Phys. Rev. B **84**, 024417 (2011).
[23]U. R. Singh, S. Chaudhuri, R. C. Budhani, and A. K. Gupta, J. Phys.: Condens. Matter **21**, 355001 (2009).
[24]M. Fath, S. Freisem, A. A. Menovsky, Y. Tomioka, J. Aarts, and J. A. Mydosh, Science **285**, 1540 (1999).
[25]T. Becker, C. Streng, Y. Luo, V. Moshnyaga, B. Damaschke, N. Shannon, and K. Samwer, Phys. Rev. Lett. **89**, 237203 (2002).
[26]J. X. Ma, D. T. Gillespie, E. W. Plummer, and J. Shen, Phys. Rev. Lett. **95**, 237210 (2005).
[27]Ch. Renner, G. Aeppli, B.-G. Kim, Y.-A. Soh, and S. W. Cheong, Nature **416**, 518 (2002).
[28]S. Seiro, Y. Fasano, I. Maggio-Aprile, E. Koller, O. Kuffer, and O. Fischer, Phys. Rev. B **77**, 020407R (2008).